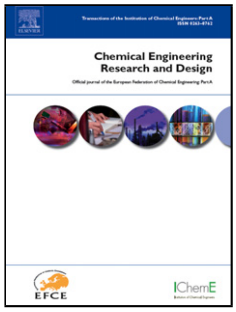

Title: On the effect of turbulence models on CFD simulations of a counter-current spray drying process

Authors: Hasan Jubaer, Sepideh Afshar, Jie Xiao, Xiao Dong Chen, Cordelia Selomulya, Meng Wai Woo

PII: S0263-8762(18)30604-X
DOI: https://doi.org/10.1016/j.cherd.2018.11.024
Reference: CHERD 3435

To appear in:

Received date: 7 July 2018
Revised date: 28 October 2018
Accepted date: 18 November 2018

Please cite this article as: Jubaer, Hasan, Afshar, Sepideh, Xiao, Jie, Chen, Xiao Dong, Selomulya, Cordelia, Woo, Meng Wai, On the effect of turbulence models on CFD simulations of a counter-current spray drying process.Chemical Engineering Research and Design https://doi.org/10.1016/j.cherd.2018.11.024

On the effect of turbulence models on CFD simulations of a counter-current spray drying process

Hasan Jubaer[a], Sepideh Afshar[a], Jie Xiao[b], Xiao Dong Chen[b], Cordelia Selomulya[a] and Meng Wai Woo[a]*

Hasan Jubaer[1], Sepideh Afshar[1], Jie Xiao[2], Xiao Dong Chen[2], Cordelia Selomulya[1], Meng Wai Woo[1*]

[a]*Department of Chemical Engineering, Faculty of Engineering, Monash University, Victoria, Australia;*

[b]*Suzhou Key Laboratory of Green Chemical Engineering, School of Chemical and Environmental Engineering, College of Chemistry, Chemical Engineering and Materials Science, Soochow University, Suzhou, Jiangsu Province 215123, China*

[1]Department of Chemical Engineering, Faculty of Engineering, Monash University, Victoria, Australia
[2]Suzhou Key Laboratory of Green Chemical Engineering, School of Chemical and Environmental Engineering, College of Chemistry, Chemical Engineering and Materials Science, Soochow University, Suzhou, Jiangsu Province 215123, China

*Corresponding author: meng.woo@monash.edu, +61 3 9905 9344

Graphical abstract

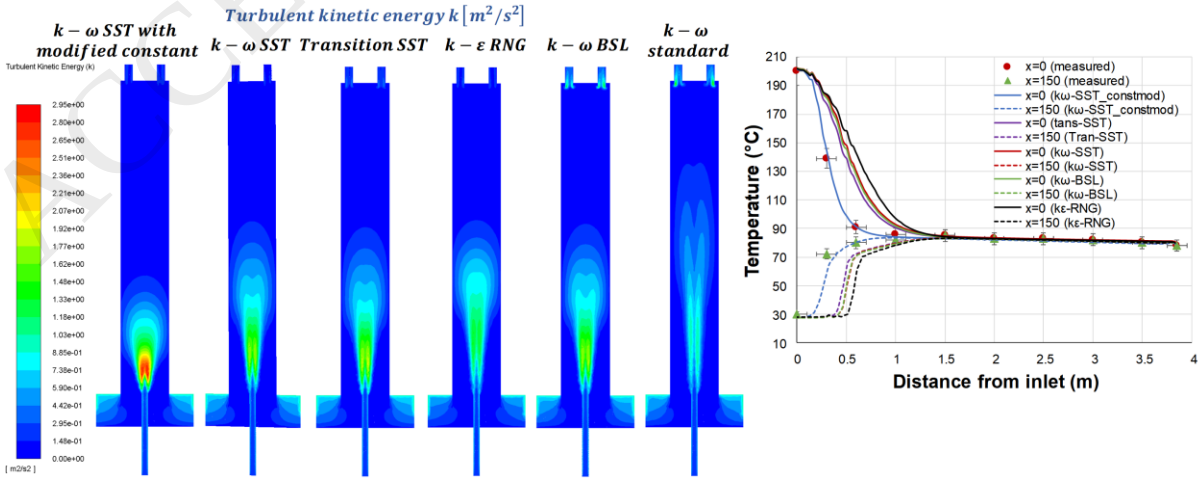

Research Highlights

- Inlet air jet potentially characterizes the air flow pattern within most spray dryers
- Increased production & dissipation of turbulence accurately captured low velocity jet shearing
- k-ω SST turbulence model manipulation led to enhanced accuracy
- Jet dissipation markedly affects the particle dispersion and hence drying history

Abstract

Accurate modeling of the flow field by means of capturing turbulence is crucial in CFD simulations. However, choosing the appropriate turbulence model remains quite challenging for simulating spray drying applications. Only a few studies have touched on this issue, although experimentally validated comparisons throughout the dryer are rare. This work aims to provide an assessment of five different turbulence models (RNG $k-\varepsilon$, standard, BSL and SST $k-\omega$ as well as transition SST) in terms of the predicted flow field throughout a lab-scale counter-current spray dryer. None of the tested models could initially provide a satisfactory match with locally measured temperatures within the chamber. The popular choice RNG $k-\varepsilon$ model led to highest discrepancies, while the $k-\omega$ variants performed only slightly better. All these models under-predicted the dissipation of the central hot air jet. Modification to the $k-\omega$ variant's characteristic constant to allow increased production of turbulence led to satisfactory agreement between the measurements and simulation results. Extended analysis revealed that different turbulence models produced significantly different drying histories. Only the $k-\omega$ SST variant with modified constant could provide predictions close to measured outlet particle moisture content and air conditions. The RNG model proved entirely unsuitable due to unrealistic results with particle injection as well. The differences in predictions among the models were attributed to different transient self-sustained air fluctuation behavior predicted within the chamber. This work will be useful in the selection of turbulence models which is fundamental to accurate CFD modeling of spray dryers.

Abbreviation

BSL	BaSeLine $k-\omega$ model
CFD	Computational Fluid Dynamics
GAB	Guggenheim-Anderson-de Boer (model)
IDF	International Dairy Federation

LES	Large Eddy Simulation
PRESTO	PREssure STaggering Option
PSD	Particle Size Distribution
RR	Rosin-Rammler distribution
RANS	Reynolds-Averaged Naviere-Stokes
REA	Reaction Engineering Approach
RNG	ReNormalization Group
RSM	Reynolds Stress Model
SAS	Scale Adaptive Simulation
SIMPLEC	Semi-Implicit Method for Pressure-Linked Equations Consistent
SST	Shear Stress Transport model
UDF	User Defined Function

Keywords: turbulence; CFD; modeling; spray drying; counter-current; flow field

Nomenclature

Latin letter

a, a_1	turbulence model constant
CD_ω	cross diffusion term (kg m^{-3} s $^{-2}$)
$d_{h,i}$	hydraulic diameter of the inlet (m)
d_D	chamber diameter (kg m^{-3} s $^{-2}$)
$F(M_t)$	compressibility function
F_1	blending function
F_2	turbulence model function
k	turbulent kinetic energy (m^{2}s^{-2})
L_D	chamber length (m)
M_{t0}	turbulence model constant
$P_K, \tilde{P}_K$	rate of production of k (kg m^{-1} s^{-3})
R_k, R_ω	turbulence model constant
Re	Reynolds number (-)
Re_i	Reynolds number at the inlet (-)
Re_D	Chamber Reynolds number (-)
Re_t	turbulent Reynolds number (-)
S	invariant measure of strain rate (s^{-1})
t	time (s)
u	velocity (m s^{-1})
y	shortest distance from the nearest wall (m)

Greek letter

$\alpha, \alpha_0, \alpha^*, \alpha_\infty, \alpha_\infty^*$	turbulence model constant
$\beta, \beta^*, \beta_i, \beta_i^*, \beta_\infty$	turbulence model constant
γ	turbulence model constant
ε	turbulent dissipation rate ($m^2\ s^{-3}$)
ζ^*	turbulence model constant
μ	dynamic molecular viscosity ($kg\ m^{-1}\ s^{-1}$)
μ_T	eddy viscosity ($kg\ m^{-1}\ s^{-1}$)
ν_T	kinematic eddy viscosity ($m^2\ s^{-1}$)
ρ	density ($kg\ m^{-3}$)
σ_k	turbulent Prandtl numbers for k (-)
σ_ω	turbulent Prandtl numbers for ω (-)
τ	shear stress ($kg\ m^{-1}\ s^{-2}$)
ω	specific turbulence dissipation rate (s^{-1})

1 Introduction

Spray drying has proven to be essential for efficient production in a wide range of industries manufacturing various products such as dairy and instant food, detergents, pharmaceuticals and agrochemicals. However, mathematically modeling this process is challenging because of its complexity, and requires interdisciplinary expertise. Moreover, obtaining detailed experimental data is difficult due to the limited accessibility to the internal of spray chambers as well as the moderately harsh conditions. Nonetheless, for such cases, Computational Fluid Dynamics (CFD) has progressively been establishing itself as the platform to simulate and better understand the phenomena involved. According to Norton and Sun (2006), CFD is employed as frequently as the traditional didactic methods of conducting experiments and mathematical modeling in solving problems involving fluid flow in both industry and science, especially because CFD offers the advantage of saving cost and time over experimentation and at the same time it is capable of overcoming the limitations of analytical solutions.

In a CFD simulation of spray drying processes, it is paramount to first capture the characteristics of the flow field, because the discrete phase (sprayed droplets) and the continuous phase (hot air) are coupled therein and thus can influence each other during the simulation. For developing the flow field, turbulence must be accurately captured, because the turbulence alongside the velocity flow field significantly affects the dispersion of the discrete phase. Moreover, the drying process was found to be directly affected by turbulence and hence could be intensified by utilizing turbulence (Southwell et al., 1999).

In the actual modeling of turbulence in spray drying simulations, various approaches have been reported. While the use of the Reynolds-averaged Navier-Stokes (RANS) framework, particularly the two-equation model closure and the Reynolds stress model (RSM) closure are most commonly employed, a trend is also observed that attempts to capture turbulence at a very fine scale, albeit the number of such works is fairly limited. For instance, there is only one report to date on the simulation of spray dryers using the Large Eddy Simulation (LES) approach (Jongsma et al., 2013) and one report using the scale adaptive simulation (SAS) approach (Fletcher and Langrish, 2009)

to turbulence modeling. It is noteworthy that both these reports were limited to air flow studies without the incorporation of sprayed droplets.

Among the two-equation turbulence models, the $k-\varepsilon$ model is perhaps the most frequently employed one. This model was first proposed by Launder and Spalding (1972) and its use became prevalent due to its numerical robustness and reasonable accuracy at an acceptable demand for computational resources. In the last fifty years, the model has been used in predicting diverse engineering flows, some of which warranted adjustments or modifications leading to different formulations in addition to the standard $k-\varepsilon$ model, such as RNG $k-\varepsilon$ (Yakhot and Orszag, 1986) and Realizable $k-\varepsilon$ (Shih et al., 1995).

In contrast to the computationally economic nature of the $k-\varepsilon$ model, the RSM approach requires seven additional transport equations for 3D cases (Huang et al., 2004). While the two-equation based RANS approach was found to be capable of capturing the spray dryer flow field (Woo, 2016), RSM may provide a higher level of detail.

While few of the CFD studies pertaining to spray drying resorted to RSM for more accurate predictions of the flow field (e.g. Ali, 2014; Ali et al., 2017; Ali et al., 2013; Bayly et al., 2004; Hernandez et al., 2018; Jaskulski et al., 2015, 2016; Wawrzyniak et al., 2017), most studies have preferred the two-equation approach, presumably due to the computational cost-performance ratio. Among the two equation models, $k-\varepsilon$ turbulence model has been widely used as the workhorse. For instance, it was shown in a review (Kuriakose and Anandharamakrishnan, 2010) of 17 to date published research works pertaining to the air flow pattern inside a spray dryer that only 2 studies chose RSM model, while the rest utilized $k-\varepsilon$ model. There are significant efforts in the literature to evaluate various forms of the $k-\varepsilon$ model for spry dryer modeling as well. The concurrent spray drying experiments undertaken in Lodz University of Technology, Poland, described in a series of report (Zbicinski et al., 2002a; Zbicinski and Piatkowski, 2004; Zbicinski et al., 2002b) provided the basis for another CFD study (Li and Zbicinski, 2005) published later, which reported that the $k-\varepsilon$ turbulence model led to the best agreement, even compared to the RSM model. It is noteworthy that in more recent CFD works (Jaskulski et al., 2015, 2016; Wawrzyniak et al., 2017) published by the same group rather RSM model was employed. Kieviet (Kieviet and Kerkhof, 1997; Kieviet et al., 1997) also provided evidence on the applicability of the $k-\varepsilon$ model with detailed experimental data of a short form cylinder-on-cone spray dryer, albeit the simulation undertaken was an axisymmetric one. Huang et al. (2004) presented a comparative study of four different turbulence models, namely the standard $k-\varepsilon$, RNG $k-\varepsilon$, Realizable $k-\varepsilon$, and RSM. They found that the Realizable $k-\varepsilon$ model was not suitable for flows involving swirl. Among the other three, RNG $k-\varepsilon$ was identified as the optimum choice with reasonable computational time and sufficient accuracy, while the RSM could provide better accuracy at the expense of significantly higher computational time and the standard $k-\varepsilon$ is less accurate for flows involving swirl. It is noteworthy that there was no detailed experimental data included in that report. Several other works (e.g. Afshar et al., 2018b; Jaskulski et al., 2017; Mezhericher et al., 2015; Tran et al., 2017; Woo et al., 2008; Woo et al., 2009b; Woo et al., 2011; Yang et al., 2015) can be found in the literature that utilized various forms of the $k-\varepsilon$ based two equation closures in order to investigate several different aspects of spray drying.

In any event, the underlying assumption in all formulations of $k-\varepsilon$ turbulence models suggests that the flow is entirely turbulent and hence the effects of molecular viscosity can be neglected in

comparison with turbulent viscosity. As a result, these models have proven to be inaccurate in predicting low velocity flows particularly in the viscous sublayers closer to the wall, despite many 'low Re' number corrections proposed to date (Menter, 2009). In general, as soon as the molecular viscosity becomes as, or more, significant than the turbulence viscosity, the predictions of $k-\varepsilon$ turbulence models start being inaccurate. Accurate prediction of such regions with low turbulence is important, particularly in the near-wall region, for instance to accurately describe the diffusion of particles in particle-wall interactions in spray dryers.

The most commonly applied alternative to the $k-\varepsilon$ turbulence models is the $k-\omega$ turbulence model, which was originally developed by Wilcox (Wilcox, 1988; Wilcox, 1993b). In addition to its simple but numerically stable nature, the $k-\omega$ model was able to provide more accurate formulations of viscous sublayers in the immediate proximity of the wall (Menter, 1994; Wilcox, 1988) as well as boundary layers in adverse pressure gradient (Wilcox, 1993a), when compared to $k-\varepsilon$ models. On the other hand, the greatest weakness of this model was the severe freestream dependency i.e. the solution was found to be strongly dependent on the specified value of ω, a limitation that was not observed with $k-\varepsilon$ models (Menter, 1992).

Considering these mutually exclusive advantages as well as disadvantages of these aforementioned two-equation models, Menter (1994) took a pragmatic approach and proposed a new formulation – Baseline (BSL) – essentially consisting of both $k-\varepsilon$ and $k-\omega$ models combined by means of a blending function. The blending function activates the $k-\omega$ model in the viscous sublayers as well as in the logarithmic region of the boundary layer, whereas it activates $k-\varepsilon$ model in the free stream region, while the different elements of these two models are gradually blended together in the intermediate region. By replacing the weak element of each model by the superior alternative offered by its counterpart, Menter ensured the robustness and accuracy in the near wall region as well as the free stream independency in the wake region.

Nevertheless, the BSL formulation still struggled to capture the onset and amount of flow separation at an adverse pressure gradient, as unlike the Reynolds Stress Model (RSM) it was unable to account for the transport of principal turbulent shear stress (Menter, 1994; Menter, 2009). In order to resolve this issue, Menter (1994), in a slightly modified version (SST) of his BSL formulation, utilized the idea originally presented by Johnson and King (1985), which was based on the assumption that the shear stress was made directly proportional to the turbulent kinetic energy (Bradshaw, 1972). With the shear stress transport was incorporated, the research group of Menter targeted the modeling of the laminar-turbulent transition in boundary layers. As an outcome of their collective effort, the transition SST model was formulated and published (Langtry et al., 2004; Menter et al., 2006; Menter et al., 2004). This was built upon the basic of SST model, with two additional transport equations – the first for the intermittency and the second for the transition onset criteria – to be solved incorporating experimental correlations to trigger the onset criteria. The authors showed that this model could be applied to a wide variety of industrial simulation problems (Menter et al., 2006).

Despite the progress made by Menter and his associates in turbulence modeling and the reported success of SST model, this model has rarely been used in simulations of spray drying. Even though the principal impetus for developing the SST model was to accurately predict boundary layers under adverse pressure gradients up to flow separation in aerodynamic simulations (Menter, 2009), the model is pertinent in many industrial flows, particularly where significant share of

boundary layers can be non-turbulent. Only a few works (Gabites et al., 2010; Kota and Langrish, 2007; Langrish et al., 2004; Malafronte et al., 2015; Ullum 2006; Ullum et al., 2010) utilizing SST models in spray dryer modeling can be found. These reports, however, were not accompanied with detailed flow field measurements to provide more evidence as the focus of the papers the development of other aspects of the CFD framework such as droplet drying, deposition modeling and protein denaturation modeling during spray drying. Although not specified, the work of Gabites et al. (2010) and the series of work by Ullum and co-workers involved industrial scale dryers, which might not have permitted detailed flow field measurements (not specifically mentioned in the papers). Only Langrish et al. (2004) mentioned that improved predictions of flow separation were obtained by the SST model over the basic $k-\varepsilon$ model. Naturally, the flow field in a spray drying chamber is a curiously diverse one, influenced by the inherent characteristics of its geometry, broad velocity spectrum depending on the scale and potential presence of sudden expansion, inlet swirl and free jet shear. These features of a spray drying chamber suggest that the assumption of a fully turbulent flow field in order to legitimize the use of the $k-\varepsilon$ model deserves further attention.

Thus, further simulation studies validated by comprehensive measurements focusing on the choice of turbulence models is needed. In this work, five different turbulence models (variants of the $k-\varepsilon$ and $k-\omega$ models) were employed to predict the flow field inside of a lab scale counter-current spray tower. The key flow characteristic in the tower investigated in this work is the dissipation of a central hot air jet into the drying chamber, which is ubiquitous in spray dryers. The models used were RNG $k-\varepsilon$, standard, BSL and SST $k-\omega$ as well as transition SST. Evaluation of the simulation results was carried out based on experimental observations and measurements within the chamber. The generic objective of this study is to improve the understanding of the effects of choosing different turbulence models for such CFD simulations.

2 Material and Methods

2.1 Description of the spray tower

The counter-current tower developed at Monash University in the Department of Chemical Engineering (Shakiba et al., 2016) was adapted for this study. The tower is 4.0 m tall and possesses a diameter of 600 mm (see **Figure 1**). The falling particles were collected on a collection tray, as these were only driven by gravity. The liquid feed was atomized at 0.5 MPa pressure through a nozzle of 0.5 mm orifice (AmFog Nozzle Technologies Inc., USA). The effective drying air was a mixture of multiple streams. The hot air was supplied by an air heater (Techspan industrial hot air blower), which was mixed with compressed air at a plenum chamber below the dryer. As the air entered the tower through the inlet near the bottom, the ambient air was entrained through the open dryer bottom. The mixture of hot and ambient air then effectively flew upwards against the falling particles and finally left the dryer, as it was sucked out by an exhaust blower. The flow rate and temperature of the drying air were therefore varied by controlling the power of the heater and ratio of the hot air to the compressed air. Additionally, by increasing the exhaust fan vacuum, the flow rate of the entrained ambient air could be increased. The drying chamber as well as the hot air inlet were insulated with glass wool, in order to inhibit the heat loss to the environment.

As expected in a counter-current spray dryer, the fine fraction of the produced powder was entrained by the ascending drying air and subsequently left the chamber through the air outlets.

This fraction was not recovered and hence was not included in our analysis specific to the powder samples. However, for thoroughness and for the readers' information, the mass of entrained particle was estimated to be slightly above 80% of the initially injected solid mass (from simulations with the preferred model). This could also be corroborated with the experimental observation.

2.2 Measurements

All the temperature measurements were performed by using K-type thermocouple probes (OMEGA Engineering inc., USA). The relative humidity was measured by means of capacitive sensors (E+E Elektronik Ges.m.b.H, Austria and Kimo Instruments, France). Pitot tubes (TSI Inc. USA) were employed to measure the air velocity and pressure. Internal temperatures were measured in 'dry run' conditions where the drying chamber was heated to steady state conditions prior to the spray of feed materials. Two sets of internal measurements were undertaken: Points 1-10 were measurements at the axis of the chamber while points 2*-9* were measurements 0.15 m off the axis of the chamber (see **Figure 1**b). The main purpose of measurements at the axis and the offset location was to understand the mixing behavior of the relatively cooler air flow which was entrained into the chamber from the bottom outer annular inlet and the central hot air jet.

The sprayed materials were distilled water and then commercial skim milk (supplier: Farmdale, ALDI Australia) having a solid content of approximately 10% for achieving the steady state with spray and the actual drying run respectively. The feed was directly transferred into the feed tank (1 L) and then kept under room temperature until the temperature of the prepared feed reached around 20°C. Then the spray was initiated.

The powder collected at the bottom outlet was immediately transferred into an airtight container and taken to moisture content analysis. The moisture content of the powder samples was determined from weight loss after drying approximately 1 g of powder in an oven at 102°C for 6 hours. The determined moisture content was cross-checked by adding some measurements obtained from a moisture analyzer (Ohaus Corporation, USA). The moisture content was confirmed by employing two methods, since due to the small amount of produced samples the prescribed amount of 3 g according to IDF Standard No.26-1964 (Pisecký, 1997) could not be maintained.

The initial droplet size distribution was estimated by conducting image analysis (ImageJ) on backlit images of a water spray shot at identical conditions as inside the spray dryer, with Phantom VEO 410 L high speed camera (Vision Research Inc., USA) and a Micro-NIKKOR 105mm f/2.8 lens (Nikon Corporation, Japan).

2.3 Model Description

2.3.1 Geometry

The unstructured mesh was created using the built-in meshing application in the ANSYS Workbench (Release 19.0). Few simplifications were made, while creating the 3D geometry used for CFD simulations. In the simplified geometry, the inserted lance (diameter 15.85 mm) for the liquid feed as well as the geometry of the nozzle were ignored eliminating such minute and fine geometries relative to the large scale of the system, to ensure numerical stability. The calculation domain was expanded 30 cm around the actual diameter towards the bottom opening of the dryer

to minimize the influence of set boundary conditions i.e. turbulence properties of the entrained air inlet on the simulation results in the actual domain. For the same reason, the hot air inlet was included along with the pipe extending up to 1 m downwards. This also helped develop reliable velocity, turbulence and temperature profiles at the actual inlet, in contrast to setting those conditions at the entrance into the chamber based on assumptions. The choice of this extension length relied upon a sensitivity analysis, which showed that at the chosen length the effect of moderate variation in set initial conditions on the predicted turbulence properties at the actual inlet was insignificant.

Higher mesh density was enforced in the vicinity of the wall as well as in the central region, in order to better capture the boundary layers of the flow-field and the impact of the jet on the flow field. **Figure 2** shows a simplified schematic of the calculation domain as well as a representative section of the mesh structure.

The final mesh had 262231 elements and 65242 nodes in total. A further increase in number of the elements did not improve the results significantly. The mesh independence was ensured through a systematic test by monitoring axial velocity and temperature predictions at various locations along the height of the spray tower.

2.3.2 Initial and Boundary Conditions

The calculation domain consists of two inlets – a mass flow inlet for the hot drying air and a pressure inlet for the entrained air – and four pressure outlets at the top. The initial and boundary conditions used are summarized in

Table 1.

2.3.3 Numerical solution

The 3-D double precision solver in ANSYS FLUENT (Release 19.0) was utilized. The spatial discretization of transport equations were all carried out in second order upwind scheme, while for pressure "PRESTO!" was used. The temporal discretization was performed in the second order implicit scheme. The pressure-velocity coupling was undertaken by SIMPLEC scheme.

The model is solved for steady state for approximately 1200 iterations until convergence was reached. Transient simulation was deemed unnecessary for flow field development, since there was no evidence suggesting any asymmetry or self-sustained oscillations in the predicted flow field (Woo, 2016). This was further verified by sequential monitoring of the velocity flow field during the steady state solution. In order to determine the convergence the reduced residual patterns ($< 1 \times 10^{-4}$) were observed alongside temperature and gas velocity magnitude at different locations distributed throughout the calculation domain. It was also ensured that the overall mass and energy balance was satisfied.

For simulation with particle injection the solution mode was switched to transient (The justification is presented later in the discussion). The transient simulation was approached through a step-by-step procedure (Woo, 2016; Woo et al., 2009b) i.e. the developed flow field obtained from the steady state solution was taken as initial condition for the transient simulation. A time step of 0.05 s was chosen to capture any oscillation that might occur with a frequency lower or equal to 20 Hz. The transient solver was run initially for around 100 time steps (dry run) until no change in residuals as well as monitored quantities was observed. Only then the particles were injected and the actual spray drying simulation was started, while two-way turbulence coupling was enabled.

Several user defined functions (UDF's) were utilized to modify some of the default features in ANSYS FLUENT solver. As it was ascertained in a previous work (Jubaer et al., 2017) by the authors that modeling non-perfect shrinkage of particles during drying is indispensable in obtaining accurate predictions regarding drying history as well as particle trajectory, the particle diameter was modified in the same way as in the cited work i.e. as a function of the current moisture content indirectly by changing the density of the discrete phase. The UDF called "`DEFINE_DPM_PROPERTY`" was employed to achieve this goal. "`DEFINE_DPM_TIMESTEP`" was switched active for limiting the time step size of the discrete phase model to $1 \times 10^{-4} s$.

In addition to capturing the shrinkage behavior the appropriate drying kinetics was accounted for by implementing the drying model Reaction Engineering Approach (REA) (Chen, 2008) through another UDF, which forced the kinetic to be accounted for during particle tracking by modifying the "vapor-particle-equilibrium". The UDF is designated "`DEFINE_DPM_VP_EQUILIB`".

In order to obtain data associated with the discrete phase, the UDF named "`DEFINE_DPM_OUTPUT`" was employed. This enabled desired data to be obtained by discrete phase sampling at different locations of the chamber under the report option in FLUENT. The statistical method of data evaluation (Woo, 2016; Yang et al., 2015) yielded average moisture content, particle size distribution and residence time. More detailed account of the UDF implementation strategy was given in the supplementary information of the cited previous work.

2.3.4 Theoretical background

Details on the RANS theoretical framework for capturing turbulent flow is established in the literature (e.g. Durbin and Reif, 2010) and is not included here for brevity. Similarly, the theoretical framework for the RNG $k-\varepsilon$ (Yakhot and Orszag, 1986), standard (Wilcox, 1993b), BSL (Menter, 1994) $k-\omega$ and transition SST (Menter et al., 2006) was not included here. Interested readers can refer to the cited literature sources. For the interest of the discussion in this manuscript, the theoretical framework for the SST $k-\omega$ is provided in brief, as this will be analyzed in greater detail in latter section of this manuscript. It is noteworthy that this SST formulation of Menter is very close to the original BSL $k-\omega$ model.

In this formulation, the turbulent kinetic energy, k and the specific dissipation rate ω, which is defined by the ratio of ε to k i.e. $\omega = \varepsilon/k$, are described by the following transport equations:

$$\frac{\partial(\rho k)}{\partial t} + \frac{\partial(\rho k u_i)}{\partial x_i} = \tilde{P}_k - \beta^* \rho k\omega + \frac{\partial}{\partial x_j}\left[\left(\mu + \frac{\mu_t}{\sigma_k}\right)\frac{\partial k}{\partial x_j}\right] \quad (1)$$

$$\frac{\partial(\rho\omega)}{\partial t} + \frac{\partial(\rho\omega u_i)}{\partial x_i} = \alpha \frac{1}{\nu_t}\tilde{P}_k - \beta\, \rho\omega^2 + \frac{\partial}{\partial x_j}\left[\left(\mu + \frac{\mu_t}{\sigma_\omega}\right)\frac{\partial \omega}{\partial x_j}\right] + 2(1-F_1)\rho\frac{1}{\sigma_{\omega,2}\omega}\frac{\partial k}{\partial x_j}\frac{\partial \omega}{\partial x_j} \quad (2)$$

σ_k and σ_ω are the turbulent Prandtl numbers for k and ω repectively and are calculated by using the blending function F_1:

$$\frac{1}{\sigma_k} = \frac{F_1}{\sigma_{k,1}} + \frac{1-F_1}{\sigma_{k,2}} \quad (3)$$

$$\frac{1}{\sigma_\omega} = \frac{F_1}{\sigma_{\omega,1}} + \frac{1-F_1}{\sigma_{\omega,2}} \quad (4)$$

The first term on the right hand side of the transport equations (1 & 2) $\tilde{P}_k$ is related to the shear tress, $\tau_{ij} = \rho\overline{u_i' u_j'}$ as given below:

$$P_k = \tau_{ij}\frac{\partial u_i}{\partial x_j} = \mu_t \frac{\partial u_i}{\partial x_j}\left(\frac{\partial u_i}{\partial x_j} + \frac{\partial u_j}{\partial x_i}\right) \quad (5)$$

$$\tilde{P}_k = \min(P_k, 10\,\beta^*\,\rho k\omega) \quad (6)$$

Combining the idea based on Bradshaw's assumption that the shear stress τ is directly proportional to the turbulent kinetic energy i.e. $\tau = \rho a_1 k$ and the description of shear stress in two-equation models i.e. $\tau = \mu_t \frac{\partial u}{\partial y}$, the shear stress was defined in the following way for conventional two-equation models:

$$\tau = \rho\sqrt{\frac{Production_k}{Dissipation_k}}a_1 k \quad (7)$$

To satisfy the relationship $\tau = \rho a_1 k$, within the framework of an eddy-viscosity model, the following limiter is added to the formulation of the turbulent viscosity:

$$\mu_t = \frac{\rho k}{\omega}\frac{1}{\max(1/\alpha^*, SF_2/a_1\omega)} \quad (8)$$

where, S is the invariant strain rate $\frac{\partial u}{\partial y}$ and F_2 is a function (see equation 10) having the value of 1 for the boundary layers and 0 for free shear layers. In an adverse pressure gradient boundary layer, production of k is larger than its dissipation leading to $S/a_1\omega > 1/\alpha^*$ and equation (8) hence

guarantees the implementation of Bradshaw's assumption, while the original formulation $\mu_t = \frac{\alpha^* \rho k}{\omega}$ is applied for the rest of the flow.

The blending function $F_1$is defined by:

$$F_1 = \tanh\left[\left\{\min\left\{\max\left(\frac{\sqrt{k}}{\beta^* \omega y}, \frac{500\mu}{\rho y^2 \omega}\right), \frac{4\rho k}{\sigma_{\omega 2} CD_{k\omega} y^2}\right\}\right\}^4\right] \tag{9}$$

$$F_2 = \tanh\left[\left\{\max\left(\frac{2\sqrt{k}}{\beta^* \omega y}, \frac{500\mu}{\rho y^2 \omega}\right)^2\right\}\right] \tag{10}$$

with

$$CD_{k\omega} = \max\left(2\rho \frac{1}{\sigma_{\omega,2}\omega} \frac{\partial k}{\partial x_j} \frac{\partial \omega}{\partial x_j}, 10^{-10}\right) \tag{11}$$

The turbulent viscosity μ_t is calculated generally via the following correlation:

$$\mu_t = \alpha^* \frac{\rho k}{\omega} \tag{12}$$

With density ρ, turbulent kinetic energy, k and specific dissipation rate, ω and the constant α, which is given as a function of turbulent Reynolds number, $Re_t = \frac{\rho k}{\mu \omega}$ by:

$$\alpha^* = \alpha^*_\infty \left(\frac{\alpha^*_0 + Re_t/R_k}{1 + Re_t/R_k}\right) \tag{13}$$

with $\alpha^*_0 = \frac{\beta_i}{3}$. The coefficient α present in the transport equation for the production of the specific dissipation rate ω is given by:

$$\alpha = \frac{\alpha_\infty}{\alpha^*} \left(\frac{\alpha_0 + Re_t/R_\omega}{1 + Re_t/R_\omega}\right) \tag{14}$$

α_∞ is calculated by means of the blending function:

$$\alpha_\infty = F_1 \alpha_{\infty,1} + (1 - F_1)\alpha_{\infty,2} \tag{15}$$

$$\alpha_{\infty,1} = \frac{\beta_{i,1}}{\beta^*_\infty} - \frac{0.41^2}{\sigma_{\omega,1}\sqrt{\beta^*_\infty}} \tag{16}$$

$$\alpha_{\infty,2} = \frac{\beta_{i,2}}{\beta^*_\infty} - \frac{0.41^2}{\sigma_{\omega,2}\sqrt{\beta^*_\infty}} \tag{17}$$

The dissipation of turbulent kinetic energy in the transport equation (1) contains the coefficient β^*, which is defined in the following manner:

$$\beta^* = \beta^*_i [1 + \zeta^* F(M_t)] \tag{18}$$

$$\beta^*_i = \beta_\infty \left(\frac{4/15 + (Re_t/R_\beta)^4}{1 + (Re_t/R_\beta)^4}\right) \tag{19}$$

The dissipation of specific dissipation rate ω in the transport equation (2) contains the coefficient β, which is defined in the following manner:

$$\beta = \beta_i \left[1 - \frac{\beta^*_i}{\beta_i} \zeta^* F(M_t)\right] \tag{20}$$

In lieu of a constant β_i value, the blending function is used to calculate it:

$$\beta_i = F_1\beta_{i,1} + (1 - F_1)\beta_{i,2} \tag{21}$$

The compressibility function $F(M_t)$ is defined as:

$$F(M_t) = \begin{cases} 0 & M_t \leq M_{t0} \\ M_t^2 - M_{t0}^2 & M_t > M_{t0} \end{cases} \tag{22}$$

With $M_t^2 = \frac{2k}{a^2}$ and $a = \sqrt{\gamma RT}$. The default model constants are defined to be $a_1 = 0.31, \alpha_\infty^* = 1, \alpha_\infty = 0.52, \alpha_0 = \frac{1}{9}, \beta_\infty^* = 0.09, \beta_i = 0.072, \beta_{i,1} = 0.075, \beta_{i,2} = 0.0828, R_\beta = 8, R_K = 6, R_\omega = 2.95, \zeta^* = 1.5, M_{t0} = 0.25$, $\sigma_{k,1} = 1.176, \sigma_{k,2} = 1.0, \sigma_{\omega,1} = 2.0, \sigma_{\omega,2} = 1.168$.

In addition to the turbulence model, in order to capture the accurate drying kinetics the Reaction Engineering Approach (REA) model (Chen, 2008) was employed, the detailed outline of which is not being included in this paper wither for brevity. The required parameters for 10% skim milk were taken from literature (Fu et al., 2011). The equilibrium moisture content was estimated by modeling the sorption isotherm of skim milk with Guggenheim-Anderson-de Boer (GAB) model with parameters reported by Lin et al. (2005).

3 Results and Discussion

3.1 Flow-field inside the chamber

A review of previous works led to the initial choice of RNG $k - \varepsilon$ model for predicting turbulence properties. Due to unavailability of appropriate equipment for accurately measuring low range velocities, the indirect method of validating the flow field by means of temperature profile was chosen. However, the predicted flow field was not in agreement with the measurements, as can clearly be seen from **Figure 3**. Particularly near the hot air inlet, where the jet is just introduced into the dryer, the temperatures were overpredicted in the center, whereas 150 mm away from the center temperatures were underpredicted. This clearly indicates an inadequate mixing of hot and cold air and thus a sustained partially unmixed flow up to 1 m above the inlet. The measurements on the other hand showed that the mixing occurred already within 0.5 m distance from the hot air inlet. Consequently, the hot and cold streams were completely mixed at a distance between 1 to 1.5 m. Similar behavior of the air flow pattern and same discrepancies between the measurements and predictions by CFD model utilizing $k - \varepsilon$ approach were observed and reported by Kieviet and Kerkhof (1997). They clearly stated that the CFD model predicted less mixing than the measurements, which made the core flatten out more rapidly in measurements as compared to the model predictions.

The reason behind the poor performance of $k - \varepsilon$ models, of which RNG is a variant, could be its well known inability to provide reliable predictions for flow field mostly governed by low Reynolds number i.e. not fully turbulent. As can be seen from the velocity flow field displayed in **Figure 4** the most of the regions in the chamber has a velocity magnitude between 0.3-1 m/s, it can be safely assumed that the flow field is mostly governed by low Reynolds number. In contrast, the studies reported in literature, in which RNG model proved to be effective, the flow field might have been considerably more turbulent dominated by swirls. The other weakness of the model,

which does not consider the transport of shear stress also contributed considerably to the deviations observed. It is expected that the impact of the shear stress transport around the free sheer flow of the hot air inlet jet on the development of the flow field would be significant.

In contrast, the predicted temperature with the $k-\omega$ variants except for the standard one provided slight improvements, however the central jet was predicted to be too long, as compared to the measured values. The largest discrepancies in case of the standard variant of the $k-\omega$ model was expected, because, as already discussed in the introduction, unlike the other variants this does not include the modifications developed by Menter to improve its performance away from the wall. **Figure 3** shows that the temperature predicted by simulations using the transition SST model was the closest to the measured values, albeit the deviation was still too significant to be ignored. Furthermore, the trends were similar among the $k-\omega$ variants.

Figure 4 shows the contour plots of the predicted velocities. From the velocity contour plots the slow decay of the inlet jet also becomes evident. Due to this slow decay, the entrained air and the central hot air remained separated and thus significantly higher temperatures were predicted in the central region of the tower, whereas in the near wall region the predicted temperature was markedly lower. It appeared, the jet dissipated much quicker in reality. The contour plots of temperature shown in **Figure 5** corroborate the identified issue.

In order to resolve this issue, further investigations into the SST-turbulence model was deemed necessary. Since the transition SST model could not provide any significant improvement over $k-\omega$ SST, this model was not chosen considering the additional computational resources required.

Since the default versions of the available models did not provide a good agreement with the measured values, as a viable alternative modifying the model constants was considered. A systematic sensitivity analysis buttressed by the study into the theoretical background of the model, revealed that, among the various model constants, $\alpha_\infty{}^*$ provided the most significant improvement in predicted results. The detailed theoretical correlations can be found in the cited sources of literature (Menter, 1994; Menter, 2009).

In the default version of the model in ANSYS Fluent the prescribed value for $\alpha_\infty{}^*$ is 1 (ANSYS® FLUENT, 2018). This value was elevated to 1.45 in this study. The rationale was to increase the turbulent viscosity, which would lead to an increased turbulent kinetic energy. Moreover, the shear stress is also proportional to the turbulent kinetic energy. The combined effect would lead to a higher turbulence at the hot air inlet among others. This would cause a faster dissipation of the jet and thus facilitate an enhanced mixing of the cold and hot stream. **Figure 6** presents the comparison among the turbulent kinetic energy profiles predicted by different turbulence model. It is clear how significantly higher the k values are for the $k-\omega$ SST model with modified constant. Additionally, the contour plots also indicate the dissipation of this high turbulence was relatively more intense than in other model cases. **Figure 6** also reveals that the predicted low and longer sustaining k values in case of $k-\varepsilon$ turbulence failed to provide satisfactory results.

The temperature profile obtained from simulations performed by using $k-\omega$ SST model with abovementioned modified constant closely matched the measurements (see **Figure 3**). The agreement was ensured not only in the central region, but also away from the jet and across the entire height of the spray tower. As a result, this variant of the turbulence model was deemed most suitable for developing an accurate flow field.

It should be noted that our aim was to find an appropriate turbulence model without increasing the computational requirement, and hence we excluded RSM from our investigation. Nonetheless, on this note, it must be mentioned here that several studies were found in the literature that observed and reported discrepancies akin to our observation despite their use of RSM model. For instance, comparison between the simulation results and detailed experimental data reported by Bayly et al. (2004) revealed disagreement in the central axis. In a recent study, Hernandez et al. (2018) employed RSM model to predict the flow pattern inside of a countercurrent spray dryer experimentally investigated by Francia et al. (2015) and reported significant lack of accuracy in the central axis as well, interestingly resembling our observation for all default turbulence models. A previous validation report of simulation results for the same spray tower conceded that the RSM model along with the realizable $R-\varepsilon$ model were only able to qualitatively predict the shape of the measured velocity profiles (Ali, 2014).

On a separate note, by making comparison with an arbitrary simulation with thermally insulated wall boundaries, the heat loss from the chamber was estimated to be approximately 1.01 kW. If divided by the corresponding surface area for the heat transfer, this value is in the same order of magnitude as the 1.53 kW of total heat loss found for another spray tower of 6 m height and 0.4 m diameter as reported by Jaskulski et al. (2017). Although direct comparison cannot be made with other dryers due to significant differences in size, geometry as well as insulation setup, the heat loss in the current tower was found to be lower than some of the reported values in the literature (e.g. total heat loss of 88 kW, 21.435 kW and a range between approximately 3.5-6 kW were reported by Harvie et al. (2002) Ali et al. (2014) and Jaskulski et al. (2015) respectively for their investigated spray towers). The relatively low heat loss in our case could be attributed to the quickly achieved mixing of the entrained and hot air, which reduced the temperature of the drying air within a short distance from the inlet, leading to a lower driving force available for heat loss to the environment for a significant portion of the drying chamber.

3.2 Drying history of particles

The discussion above clearly shows how the prediction of the flow field can significantly vary from the reality for different turbulence models. Of course, it is crucial to understand how the predicted drying of particles is affected, if these developed flow fields were used to continue the spray drying simulation. In order to investigate this issue, skim milk particles were injected in the developed flow field and the simulation was continued in a transient mode.

At this stage of the work, steady state simulations could not be continued further with particle injection, because the monitored quantities such as the velocities and temperatures at different locations started to show significant fluctuations. A similar case was reported in a previous work by the authors (Jubaer et al., 2017), where self-sustained fluctuations were instigated by the injection of the discrete phase into a precariously steady flow field. Similar to that case, there was no sign of fluctuations during the flow development without the discrete phase suggesting the suitability of a steady state solution method. However, injection of particles readily rendered the flow field into an asymmetric transient one. **Figure 7** depicts these fluctuations. It is noteworthy that all turbulence models, with the initiation of particles injection, led to the transient features. This eliminates any of the models to be the source of these disturbances. **Figure 7**a shows the fluctuations observed in velocity magnitudes at a location 3.5 m away from the inlet and **Figure**

7b presents the erratic oscillations in outlet temperature values. It was found that the asymmetry in flow field and fluctuations were more pronounced in the vicinity of the atomizer irrespective of the applied turbulence model. At positions away from the atomizer, the fluctuations were fairly negligible to non-existent. The velocity vectors as well as temperature contour shown in **Figure 8** clearly depicts the asymmetry present near the outlet, while the jet as well as the flow around the air inlet (bottom if the dryer) remains unaffected. A discussion specifically pertaining to the source of such transient features in an initially predicted steady flow field was recently presented elsewhere (Afshar et al., 2018a). By eliminating the possible influence of the physical geometry, meshing and mathematical model in the discussion, the seed for or the instigation of 'numerical' self-sustained fluctuation was attributed to numerical imbalance during the solution of the flow field. Such numerical imbalance may indeed propagate into imbalances predicted in the physical flow field, building up the potential for self-sustained fluctuations. Perhaps the numerical coupling with particles introduced into the simulation as well indeed contribute to such instability, as observed here or elsewhere (Jubaer et al., 2017). Whether or not such imbalances propagate into self-sustained flow behaviour certainly depends on the propensity of the spray drying chamber for 'dampening' such physical or numerical imbalances. At any rate, it must be noted here that the understanding on the numerical source of self-sustained fluctuation is extremely important in guiding the numerical approach employed in the CFD simulation of spray dryers.

Furthermore, from **Figure 7** it becomes very evident that the velocity and temperature predicted by $k-\varepsilon$ RNG was fairly erratic. In order to understand this discrepancy we have to refer to the flow behaviour ascertained in the earlier discussion regarding the sustained incoming jet for a longer length scale and the lack of shear stress transport. **Figure 9** also provides some more insight. It can be seen that the cold patch due to evaporation turned to one side practically building a channel for the hot air to escape without having proper contact with the particles. The particles were more likely to take the path away from hot air stream. In the course of the simulation, this cold patch moved around from one extreme to the other (an example is shown in **Figure 9**a right next to the 50s snapshot and a solution animation video can be found online, see Video 1). This phenomenon can be attributed to the longer central jet, which was practically influencing and forcing the spray to move away from the centre to either of the sides. At any rate, this introduced considerable amount of fluctuations, ultimately leading to near divergence. The divergence might be avoided by choosing a very fine time step, however significantly erratic predictions (as compared and shown in **Figure 7**) proved fairly unrealistic, since they were never encountered during the measurements. This observed failure of $k-\varepsilon$ RNG model in providing reliable results indicated that this model is not suitable for application in this case.

Investigations into the drying behaviour of the particle with respect to different turbulence models revealed that the drying history and hence the predicted final moisture content was significantly affected by the flow field predicted by different turbulence models. From

Table 2, it can be clearly seen that the mass average moisture contents differ markedly. The closest agreement with measured data was found with the previously chosen $k-\omega$ SST with modified constants. The default $k-\omega$ SST model performs relatively better than the $k-\varepsilon$ RNG model. However, it is noteworthy that both of the models overpredicts the final moisture content. This can be explained by the flow field described earlier (shown in **Figure 4** thru **Figure 6**). Since only in the $k-\omega$ SST model with modified constant, the hot and cold air streams were mixed very early leading to a homogeneously distributed higher temperature sustaining in most part of the dryer as compared to the field predicted by the other default two-equation models, the effective driving force for transferring heat and mass was higher for the particles. This ultimately led to enhanced drying. In contrast, unmixed air streams exposed a fraction of the injected particles to a higher driving force for a shorter period of time, while leaving the rest falling through a cooler ambient causing poor drying. The distributions of moisture content in particles sampled at the outlet, which was shown in **Figure 10**, also corroborate this theory. All of the models predicted the highest percentage of particles under 5% rest moisture content, while the chosen $k-\omega$ SST with modified constants predicted these to be over 90%. The rank of predicted percentages of particles at higher moisture contents than the average was reversed for the models, which in effect caused the average moisture content to soar for other two default models. The presence of poorly dried large and heavy particles actually increases the mass-weighted average moisture content, whereas the effect of higher mass would be ignored in simple number based average. The failure to predict realistic results by $k-\varepsilon$ RNG can be explained by the observation described above in association with **Figure 9**. The resulting poor contact time with hot air and channel flow due to the distinctive flow field resulted in poor heat and mass transfer. Consequently, the particles, particularly the heavier ones retained moisture quite markedly (see green and red particles in **Figure 9** closer to the powder outlet).

Furthermore, the increased production of turbulent kinetic energy as well as enhanced dissipation in case of the best performing $k-\omega$ SST with modified constants must have contributed to the increased drying, as Southwell et al. (1999) showed that turbulence intensifies the drying process.

Comparing with the measured values for average moisture content and outlet air conditions (shown in

Table 2) showed again that $k-\omega$ SST with modified constants could provide predictions closest to the experimentally determined values. The default $k-\omega$ SST again performed better than the $k-\varepsilon$ RNG model, however it could not agree as well as that with modified constant.

It is noteworthy that this effect of choosing the turbulence models on the predicted drying became evident because of the operating parameters applied here. It is obvious that a lower rate of atomization or higher inlet air temperature or longer height leading to higher residence time of the particles would help disguise this effect, if only the outlet conditions were analysed. The residence time and operating temperature at the employed counter-current spray dryer unravelled this very important phenomenon, which may occur in every spray dryer. The implication of overpredicting the moisture content in particles by simulation as a result of choosing the wrong turbulence model could lead to poor design decisions or flawed changes in operation leading to inefficient drying.

3.3 Comparison with other studies

Before concluding this work, to put this work into perspective it is of interest to compare the investigated spray dryer in this work with some other simulated dryers in the literature so that a possible correlation can be pursued. In

Table 3 such a comparison is presented. Since dryer geometry and operating conditions are fairly different each case, it is challenging to find a common platform to compare the results. Therefore, we calculated some dimensionless quantities to serve this purpose. Alongside the aspect ratio (chamber length to diameter) and expansion ratio (chamber diameter to inlet hydraulic diameter), the average global Reynolds number with respect to the chamber and the Reynolds number at the inlet are calculated.

At first by examining alone the average Reynolds number with respect to the chamber it can be said that no trend can be recognized. However this combined with the Reynolds number at the inlet (since the area closer to the inlet proved to be the most difficult to predict), it can be ascertained that our investigated spray dryer is among the ones exhibiting relatively low Reynolds number. This was mentioned earlier in the discussion to refer to one of the reasons behind the poor performance of $k-\varepsilon$ turbulence model. In addition, the similar order of magnitudes of the calculated Reynolds number indicates that this study is comparable to other studies reported in the literature and hence the findings can be utilized for a broad spectrum of spray dryers.

However, considering the highest discrepancies particularly closer to the central axis and the inlet air jet, when we turned to the expansion ratios of the investigated dryers, we can see that the only study that exhibited accurate prediction with $k-\varepsilon$ model, did not have any incoming air jet dissipating into the larger chamber. The studies having relatively high expansion ratio either resorted to other turbulence models such as RSM and $k-\omega$ SST or accepted the resulting deviations (reviewed in detail in the Introduction). Therefore, from the comparison it may be concluded that spray dryers with inlet jets, which dissipate in the expanded chamber are more demanding for $k-\varepsilon$ model to predict accurately. This is expected, since it is well known that $k-\varepsilon$ model does not account for the transport of shear stress. The highest deviation occurs at the locations closer to the jet, whereas the locations away from it as well as outlet conditions may be well predicted. While RSM or $k-\omega$ SST models appear to perform better in that regard, manipulating the model constants may lead to enhanced accuracy, as shown in this work.

One significant difference between the investigated spray dryer and the reported spray dryers in the literature, specially discussed in

Table 3, is the presence of the entrained ambient air, which mixed with the supplied hot drying air. The air entrainment ratio i.e. the ratio of the mass flow rate of entrained air to that of the total drying air was calculated to be approximately 65%. The entrained air provided us with the opportunity to investigate the effect of the chosen turbulence model on the mixing of these two different air streams. While other dryers may not have this exact configuration, the fundamental fluid flow phenomenon here, which is the shearing and mixing of the central air jet, can be applied to other spray drying operation.

4 Conclusions

In this work, five different turbulence models were assessed in CFD simulations of a lab scale counter-current spray drying process. Steady state simulation results were first compared with experimental data. Initially no satisfactory agreement could be achieved with the default versions of these models. It was also ascertained that using the RNG $k-\varepsilon$ model led to the highest deviations from the measured values. The $k-\omega$ variants performed slightly better, but still made unsatisfactory predictions. Therefore, the model constants needed minor modifications. This finally led to a more satisfactory agreement between the measurements and simulation results.

From this work, it can be concluded that the tested turbulence models with default settings are unlikely to provide a good agreement between the simulation and measured data, particularly for a lab scale dryer, where the flow field might not be entirely turbulent, despite the available low Reynold number corrections. Contrary to common practice, $k-\varepsilon$ models might not be appropriate for simulations involving such dryers. As alternative, $k-\omega$ variants of turbulence models, especially the SST model, perform slightly better. It is noteworthy that the detailed flow field behavior such as local temperature, pressure and velocity are most likely to deviate significantly from the reality, particularly at the vicinity of any source of turbulence e.g. inlet jets, even though the overall conditions may match with experimental data. Furthermore, this work demonstrated the relationship between the production of turbulent kinetic energy and the jet behavior. It was ascertained that if an incoming jet is observed to dissipate very quickly in a short length scale facilitating enhanced mixing of two disparate flow streams, the default turbulence model has to be modified to produce an elevated turbulent kinetic energy as well as diffusivity.

Investigations into the effect of different turbulence models on the predictions of drying performance showed that predicted flow field considerably influences the particle drying history, as expected. The $k-\omega$ SST model with modified constant, which could match the experimental flow field the best, predicted the final moisture content of the particles as well as outlet air conditions providing the best agreement with experimental results, while the default $k-\omega$ SST and $k-\varepsilon$ RNG models markedly overpredicted the moisture content. The overprediction can be attributed to the unmixed cold streams and the hot free shear jet, which expose the particles to different driving force for heat and mass transfer. This ultimately leaves some large poorly dried particles that drive the average moisture high. Again in terms of predicting the drying history, among the tested models the $k-\varepsilon$ RNG model performed the worst and proved to be unsuitable for application for similar flow field. Additionally, it was observed during the simulations with the RNG model that the longer sustaining jet can ultimately force the spray to sway from side to side and thus cause flow field instability. This may also lead to poor heat and mass transfer between the drying air and the particles.

The work also supported the observation made by the authors elsewhere that the injection of particles into a barely steady flow field can result in transient features i.e. self-sustained oscillations requiring transient simulations in lieu of steady state ones. This observation is extremely important, because according to common practice, the decision of choosing between the steady and the transient method of simulation usually relies upon the initial simulation results for flow field development excluding the discrete phase, if at all.

This work will prove extremely useful in simulating spray drying applications in lab scale as well as industrial spray dryers, since the choice of an appropriate turbulence model can considerably improve the accuracy of the prediction. This will also be crucial in the application of CFD simulations in designing a new spray dryer or making changes in operations for existing spray dryers. Future work should include similar investigations into different scales and geometries of spray dryers. The comparison should consider more advanced and detailed methods such as scale adaptive simulation (SAS), large eddy simulation (LES) with the perspective of weighing the level of accuracy and need for computational resources. This will enable the suitability of existing turbulence models to be better understood and perhaps a novel and more accurate turbulence model to be developed for generic cases or at least particularly for spray drying applications.

Acknowledgement

This project is supported by the Australian Government Department of Industry, Innovation, and Science through the Australia-China Science and Research Fund (ACSRF48154), and is conducted as part of the research program of the Australia-China Joint Research Centre in Future Dairy Manufacturing (http://acjrc.eng.monash.edu/). Soochow University acknowledges The National Key Research and Development Program of China (International S&T Cooperation Program, ISTCP, 2016YFE0101200) for support of the Australia-China collaboration.

5 References

Afshar, S., Jubaer, H., Chen, B., Xiao, J., Chen, X.D., Woo, M.W., 2018a. Computational fluid dynamics simulation of spray dryers: transient or steady state simulation?, 21st International Drying Symposium (IDS 2018), València, Spain.

Afshar, S., Metzger, L., Patel, H., Selomulya, C., Woo, M.W., 2018b. A practical CFD modeling approach to estimate outlet boundary conditions of industrial multistage spray dryers: Inert particle flow field investigation. Drying Technology, 1-15, https://doi.org/10.1080/07373937.2018.1464473.

Ali, M., 2014. Numerical Modeling of a Counter-Current Spray Drying Tower, School of Chemical and Process Engineering. The University of Leeds.

Ali, M., Mahmud, T., Heggs, P.J., Ghadiri, M., Bayly, A., Ahmadian, H., Martin de Juan, L., 2017. CFD modeling of a pilot-scale countercurrent spray drying tower for the manufacture of detergent powder. Drying Technology 35, 281-299, https://doi.org/10.1080/07373937.2016.1163576.

Ali, M., Mahmud, T., Heggs, P.J., Ghadiri, M., Djurdjevic, D., Ahmadian, H., Juan, L.M.d., Amador, C., Bayly, A., 2014. A one-dimensional plug-flow model of a counter-current spray drying tower. Chemical Engineering Research and Design 92, 826-841, https://doi.org/10.1016/j.cherd.2013.08.010.

Ali, M., Mahmud, T., Heggs, P.J., Ghadiri, M., Francia, V., Bayly, A., Djurdjevic, D., Ahmadian, H., Martin, L., 2013. CFD modeling of a counter-current spray drying tower, 8th International conference on Multiphase Flow (ICMF 2013), Jeju, South Korea.

ANSYS® FLUENT, 2018. Help System, ANSYS FLUENT Theory Guide, Release 19.0. ANSYS, Inc., U.S.A.

Bayly, A.E., Jukes, P., Groombridge, M., McNally, C., 2004. Airflow patterns in a counter-current spray drying tower-simulation and measurement, Proceedings of the 14th International Drying Symposium, pp. 775-781.

Bradshaw, P., 1972. The understanding and prediction of turbulent flow. The Aeronautical Journal (1968) 76, 403-418, https://doi.org/10.1017/S0001924000043360.

Chen, X.D., 2008. The Basics of a Reaction Engineering Approach to Modeling Air-Drying of Small Droplets or Thin-Layer Materials. Drying Technology 26, 627-639, https://doi.org/10.1080/07373930802045908.

Durbin, P.A., Reif, B.A.P., 2010. Statistical Theory and Modeling for Turbulent Flows, 2nd ed. John Wiley & Sons, Ltd.

Fletcher, D.F., Langrish, T.A.G., 2009. Scale-adaptive simulation (SAS) modeling of a pilot-scale spray dryer. Chemical Engineering Research and Design 87, 1371-1378, https://doi.org/10.1016/j.cherd.2009.03.006.

Francia, V., Martin, L., Bayly, A.E., Simmons, M.J.H., 2015. Influence of wall friction on flow regimes and scale-up of counter-current swirl spray dryers. Chemical Engineering Science 134, 399-413, https://doi.org/10.1016/j.ces.2015.04.039.

Fu, N., Woo, M.W., Lin, S.X.Q., Zhou, Z., Chen, X.D., 2011. Reaction Engineering Approach (REA) to model the drying kinetics of droplets with different initial sizes—experiments and analyses. Chemical Engineering Science 66, 1738-1747, https://doi.org/10.1016/j.ces.2011.01.009.

Gabites, J.R., Abrahamson, J., Winchester, J.A., 2010. Air flow patterns in an industrial milk powder spray dryer. Chemical Engineering Research and Design 88, 899-910, https://doi.org/10.1016/j.cherd.2009.12.009.

Harvie, D.J.E., Langrish, T.A.G., Fletcher, D.F., 2002. A Computational Fluid Dynamics Study of a Tall-Form Spray Dryer. Food and Bioproducts Processing 80, 163-175, https://doi.org/10.1205/096030802760309188.

Hernandez, B., Fraser, B., Martin de Juan, L., Martin, M., 2018. Computational Fluid Dynamics (CFD) Modeling of Swirling Flows in Industrial Counter-Current Spray-Drying Towers under Fouling Conditions. Industrial & Engineering Chemistry Research 57, 11988-12002, https://doi.org/10.1021/acs.iecr.8b02202.

Huang, L., Kumar, K., Mujumdar, A.S., 2004. Simulation of a Spray Dryer Fitted with a Rotary Disk Atomizer Using a Three-Dimensional Computional Fluid Dynamic Model. Drying Technology 22, 1489-1515, https://doi.org/10.1081/DRT-120038737.

Jaskulski, M., Atuonwu, J.C., Tran, T.T.H., Stapley, A.G.F., Tsotsas, E., 2017. Predictive CFD modeling of whey protein denaturation in skim milk spray drying powder production. Advanced Powder Technology 28, 3140-3147, https://doi.org/10.1016/j.apt.2017.09.026.

Jaskulski, M., Wawrzyniak, P., Zbiciński, I., 2015. CFD Model of Particle Agglomeration in Spray Drying. Drying Technology 33, 1971-1980, https://doi.org/10.1080/07373937.2015.1081605.

Jaskulski, M., Wawrzyniak, P., Zbiciński, I., 2016. CFD prediction of powder particle size distribution in the industrial scale spray drying process, The 20th International Drying Symposium (IDS 2016) Gifu, Japan.

Johnson, D.A., King, L.S., 1985. A mathematically simple turbulence closure model for attached and separated turbulent boundary layers. AIAA Journal 23, 1684-1692, https://doi.org/10.2514/3.9152.

Jongsma, F.J., Innings, F., Olsson, M., Carlsson, F., 2013. Large eddy simulation of unsteady turbulent flow in a semi-industrial size spray dryer. Dairy Science & Technology 93, 373-386, https://doi.org/10.1007/s13594-012-0097-y.

Jubaer, H., Afshar, S., Xiao, J., Chen, X.D., Selomulya, C., Woo, M.W., 2017. On the importance of droplet shrinkage in CFD-modeling of spray drying. Drying Technology, 1-17, https://doi.org/10.1080/07373937.2017.1349791.

Kieviet, F.G., Kerkhof, P.J.A.M., 1997. Air flow, temperature and humidity patterns in a co-current spray dryer: modeling and measurements. Drying Technology 15, 1763-1773, https://doi.org/10.1080/07373939708917325.

Kieviet, F.G., Van Raaij, J., De Moor, P.P.E.A., Kerkhof, P.J.A.M., 1997. Measurement and Modeling of the Air Flow Pattern in a Pilot-Plant Spray Dryer. Chemical Engineering Research and Design 75, 321-328, https://doi.org/10.1205/026387697523778.

Kota, K., Langrish, T., 2007. Prediction of Deposition Patterns in a Pilot-Scale Spray Dryer Using Computational Fluid Dynamics (CFD) Simulations, Chemical Product and Process Modeling.

Kuriakose, R., Anandharamakrishnan, C., 2010. Computational fluid dynamics (CFD) applications in spray drying of food products. Trends in Food Science & Technology 21, 383-398, https://doi.org/https://doi.org/10.1016/j.tifs.2010.04.009.

Langrish, T.A.G., Williams, J., Fletcher, D.F., 2004. Simulation of the Effects of Inlet Swirl on Gas Flow Patterns in a Pilot-Scale Spray Dryer. Chemical Engineering Research and Design 82, 821-833, https://doi.org/10.1205/0263876041596661.

Langtry, R.B., Menter, F.R., Likki, S.R., Suzen, Y.B., Huang, P.G., Völker, S., 2004. A Correlation-Based Transition Model Using Local Variables—Part II: Test Cases and Industrial Applications. Journal of Turbomachinery 128, 423-434, https://doi.org/10.1115/1.2184353.

Launder, B.E., Spalding, D.B., 1972. Lectures in mathematical models of turbulence. Academic Press, London, New York,.

Li, X., Zbicinski, I., 2005. A Sensitivity Study on CFD Modeling of Cocurrent Spray-Drying Process. Drying Technology 23, 1681-1691, https://doi.org/10.1081/DRT-200065093.

Lin, S.X.Q., Chen, X.D., Pearce, D.L., 2005. Desorption isotherm of milk powders at elevated temperatures and over a wide range of relative humidity. Journal of Food Engineering 68, 257-264, https://doi.org/10.1016/j.jfoodeng.2004.05.036.

Malafronte, L., Ahrné, L., Innings, F., Jongsma, A., Rasmuson, A., 2015. Prediction of regions of coalescence and agglomeration along a spray dryer—Application to skim milk powder. Chemical Engineering Research and Design 104, 703-712, https://doi.org/10.1016/j.cherd.2015.10.011.

Menter, F.R., 1992. Influence of freestream values on k-omega turbulence model predictions. AIAA Journal 30, 1657-1659, https://doi.org/10.2514/3.11115.

Menter, F.R., 1994. Two-equation eddy-viscosity turbulence models for engineering applications. AIAA Journal 32, 1598-1605, https://doi.org/10.2514/3.12149.

Menter, F.R., 2009. Review of the shear-stress transport turbulence model experience from an industrial perspective. International Journal of Computational Fluid Dynamics 23, 305-316, https://doi.org/10.1080/10618560902773387.

Menter, F.R., Langtry, R., Völker, S., 2006. Transition Modeling for General Purpose CFD Codes. Flow, Turbulence and Combustion 77, 277-303, https://doi.org/10.1007/s10494-006-9047-1.

Menter, F.R., Langtry, R.B., Likki, S.R., Suzen, Y.B., Huang, P.G., Völker, S., 2004. A Correlation-Based Transition Model Using Local Variables—Part I: Model Formulation. Journal of Turbomachinery 128, 413-422, https://doi.org/10.1115/1.2184352.

Mezhericher, M., Levy, A., Borde, I., 2015. Multi-Scale Multiphase Modeling of Transport Phenomena in Spray-Drying Processes. Drying Technology 33, 2-23, https://doi.org/10.1080/07373937.2014.941110.

Norton, T., Sun, D.-W., 2006. Computational fluid dynamics (CFD) – an effective and efficient design and analysis tool for the food industry: A review. Trends in Food Science & Technology 17, 600-620, https://doi.org/10.1016/j.tifs.2006.05.004.

Pisecký, J., 1997. Handbook of Milk Powder Manufacture. GEA Process Engineering A/S (GEA Niro), Copenhagen, Denmark.

Shakiba, S., Mansouri, S., Selomulya, C., Woo, M.W., 2016. In-situ crystallization of particles in a counter-current spray dryer. Advanced Powder Technology 27, 2299-2307, https://doi.org/10.1016/j.apt.2016.07.001.

Shih, T.-H., Liou, W.W., Shabbir, A., Yang, Z., Zhu, J., 1995. A new k-ϵ eddy viscosity model for high reynolds number turbulent flows. Computers & Fluids 24, 227-238, https://doi.org/10.1016/0045-7930(94)00032-T.

Southwell, D.B., Langrish, T.A.G., Fletcher, D.F., 1999. Process Intensification in Spray Dryers by Turbulence Enhancement. Chemical Engineering Research and Design 77, 189-205, https://doi.org/10.1205/026387699526098.

Tran, T.T.H., Jaskulski, M., Tsotsas, E., 2017. Reduction of a model for single droplet drying and application to CFD of skim milk spray drying. Drying Technology 35, 1571-1583, https://doi.org/10.1080/07373937.2016.1263204.

Ullum , T., 2006. Simulation of a spray dryer with a rotary atomizer: The appearance of vortex breakdown, Proceedings of the 15th International Drying Symposium (IDS 2006), Budapest, Hungary, pp. 251 – 257.

Ullum, T., Sloth, J., Brask, A., Wahlberg, M., 2010. Predicting Spray Dryer Deposits by CFD and an Empirical Drying Model. Drying Technology 28, 723-729, https://doi.org/10.1080/07373931003799319.

Wawrzyniak, P., Jaskulski, M., Zbiciński, I., Podyma, M., 2017. CFD modeling of moisture evaporation in an industrial dispersed system. Advanced Powder Technology 28, 167-176, https://doi.org/10.1016/j.apt.2016.09.029.

Wilcox, D.C., 1988. Reassessment of the scale-determining equation for advanced turbulence models. AIAA Journal 26, 1299-1310, https://doi.org/10.2514/3.10041.

Wilcox, D.C., 1993a. Comparison of two-equation turbulence models for boundary layers with pressure gradient. AIAA Journal 31, 1414-1421, https://doi.org/10.2514/3.11790.

Wilcox, D.C., 1993b. Turbulence modeling for CFD. DCW industries La Canada, CA.

Woo, M.-W., Daud, W.R.W., Tasirin, S.M., Talib, M.Z.M., 2009a. Controlling food powder deposition in spray dryers: Wall surface energy manipulation as an alternative. Journal of Food Engineering 94, 192-198, https://doi.org/10.1016/j.jfoodeng.2008.10.001.

Woo, M.W., 2016. Computational Fluid Dynamics Simulation of Spray Dryers: An Engineer's Guide. CRC Press, Boca Raton London New York.

Woo, M.W., Daud, W.R.W., Mujumdar, A.S., Wu, Z., Meor Talib, M.Z., Tasirin, S.M., 2008. CFD Evaluation of Droplet Drying Models in a Spray Dryer Fitted with a Rotary Atomizer. Drying Technology 26, 1180-1198, https://doi.org/10.1080/07373930802306953.

Woo, M.W., Daud, W.R.W., Mujumdar, A.S., Wu, Z., Talib, M.Z.M., Tasirin, S.M., 2009b. Non-Swirling Steady and Transient Flow Simulations in Short-Form Spray Dryers. Chemical Product and Process Modeling 4, Article 20, https://doi.org/10.2202/1934-2659.

Woo, M.W., Rogers, S., Lin, S.X.Q., Selomulya, C., Chen, X.D., 2011. Numerical probing of a low velocity concurrent pilot scale spray drying tower for mono-disperse particle production – Unusual characteristics and possible improvements. Chemical Engineering and Processing: Process Intensification 50, 417-427, https://doi.org/
10.1016/j.cep.2011.02.007.

Yakhot, V., Orszag, S.A., 1986. Renormalization group analysis of turbulence. I. Basic theory. Journal of Scientific Computing 1, 3-51, https://doi.org/10.1007/bf01061452.

Yang, X., Xiao, J., Woo, M.-W., Chen, X.D., 2015. Three-Dimensional Numerical Investigation of a Mono-Disperse Droplet Spray Dryer: Validation Aspects and Multi-Physics Exploration. Drying Technology 33, 742-756, https://doi.org/10.1080/07373937.2014.990565.

Zbicinski, I., Delag, A., Strumillo, C., Adamiec, J., 2002a. Advanced experimental analysis of drying kinetics in spray drying. Chemical Engineering Journal 86, 207-216, https://doi.org/10.1016/S1385-8947(01)00291-1.

Zbicinski, I., Piatkowski, M., 2004. Spray Drying Tower Experiments. Drying Technology 22, 1325-1349, https://doi.org/10.1081/DRT-120038732.

Zbicinski, I., Strumillo, C., Delag, A., 2002b. Drying kinetics and particle residence time in spray drying. Drying Technology 20, 1751-1768, https://doi.org/10.1081/DRT-120015412.

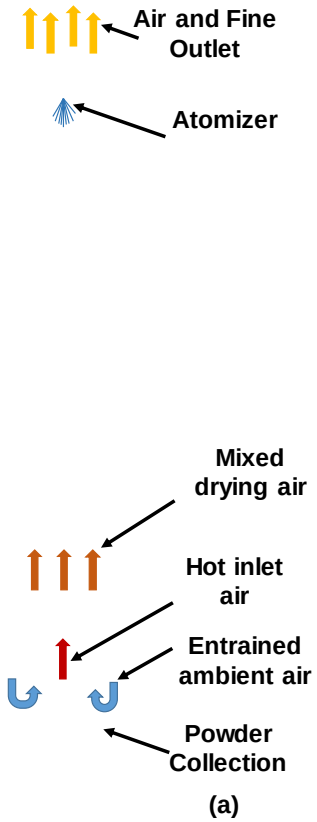

Measurements:

1: T, RH, P
2-9: T
2*-9*: T
10: T, RH, P
11: T, RH
12: Powder sample

T=Temperature
RH=Relative humidity
P=Pressure

(b)

Figure 1: *(a) Schematic illustration of the counter-current spray dryer developed at Monash University. (b) conducted measurements during spray drying run and their corresponding positions marked on the schematic drawing of the dryer.*

Figure 2: *Cross-sectional view of the mesh used (rotated 90° anti-clockwise) in the simulations with all relevant boundaries*

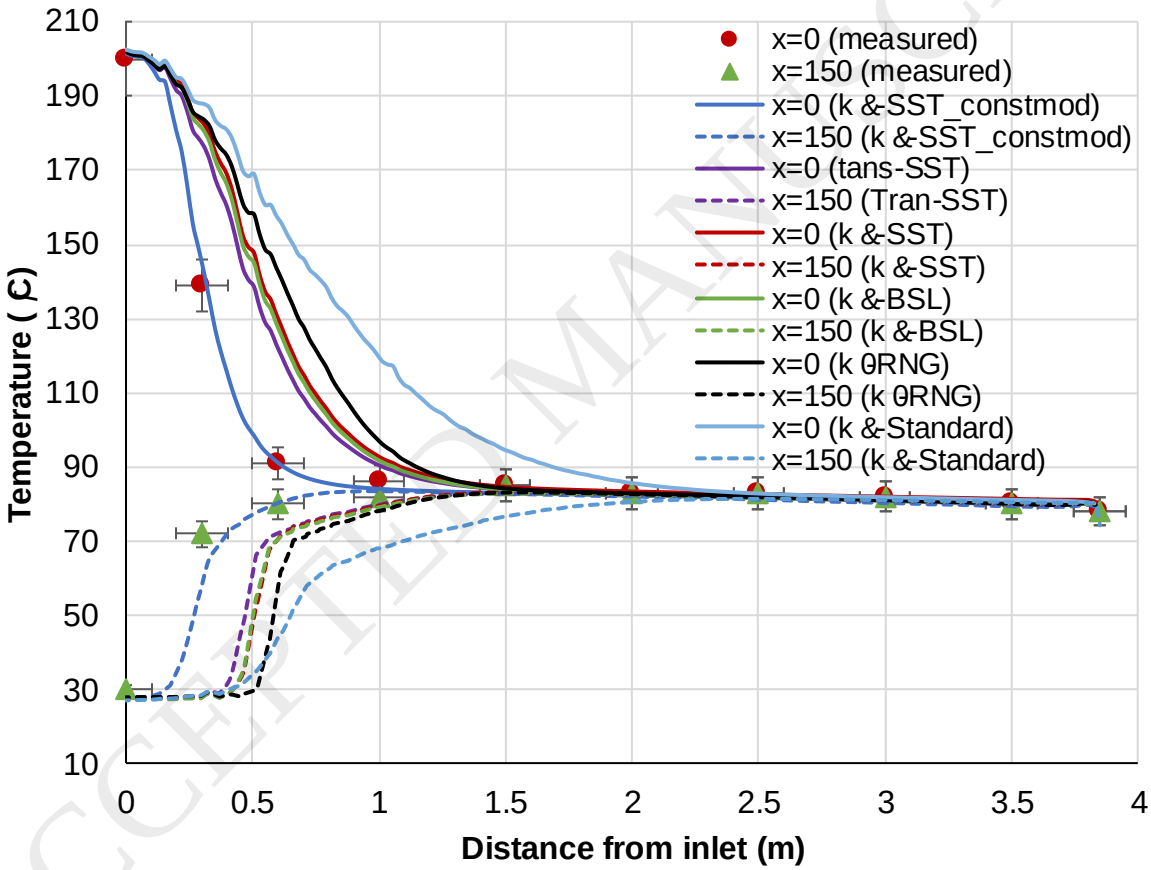

Figure 3: *Comparison of measured and predicted temperature profile at the centre axis (x=0, solid lines) and at 150 mm away from the centre axis (x=150 mm, dotted lines) along the height of the counter-current spray tower*

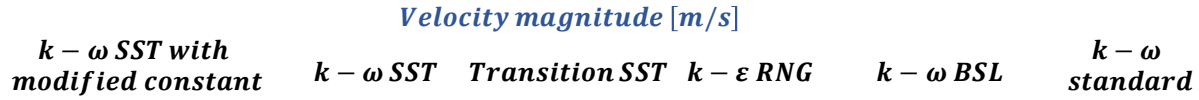

Figure 4: *Contour plots of velocity magnitude (in m/s) predicted by CFD simulations of the lab-scale counter-current dryer with different turbulence models*

Figure 5: *Contour plots of static temperature (in K) predicted by CFD simulations of the lab-scale counter-current dryer with different turbulence models*

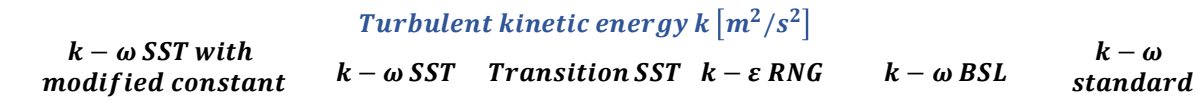

Figure 6: *Contour plots of static temperature (in K) predicted by CFD simulations of the lab-scale counter-current dryer with different turbulence models*

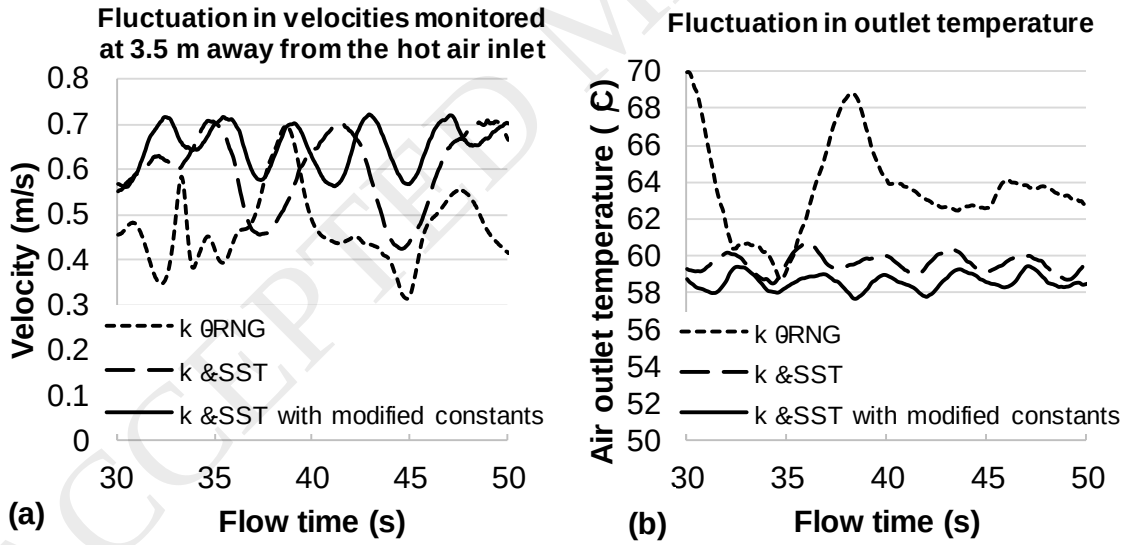

Figure 7: *Fluctuations observed in flow field variables following the particle injection (recorded values shown between the flow time 30 s and 50 s); (a) velocity magnitude of a point monitor located at 3.5 m above the hot air inlet, (b) the air outlet temperature.*

***Figure 8**: Snapshot of the transient flow field after a flow time of 50 s with particle injection. Velocity vectors (on the left) and contour plots of temperature (right) shown on the plane z=0 were both predicted with k-ω SST turbulence models with modified constant.*

(a) (b) (c)

***Figure 9**: Snapshot of the transient flow field after a flow time of 50 s with particle injection. (a) Temperature contour plot at 50s (left) and another snapshot of the other extreme position*

(right) at a different flow time, (b) velocity vectors and (c) tracked particles colored by their moisture content shown on the plane z=0 were predicted with k-ε RNG turbulence model.

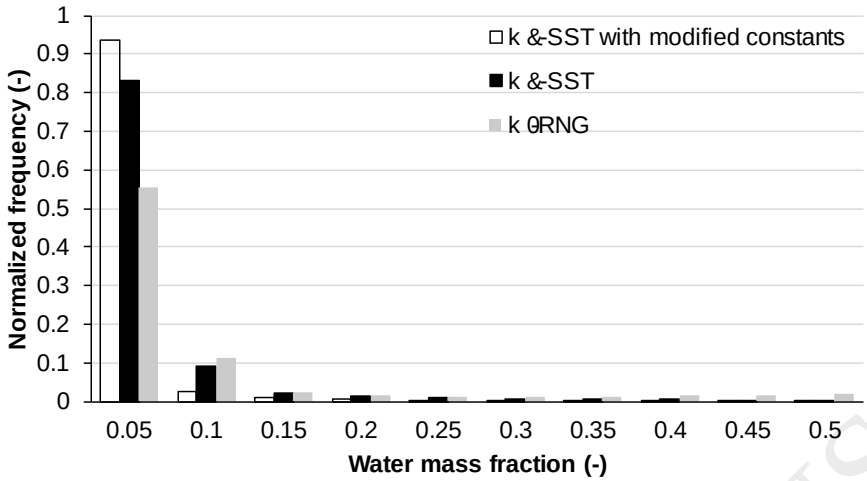

***Figure 10**: Comparison of mass-weighted moisture content distribution in particles sampled at the bottom outlet of the chamber during the flow time 30 s and 50 s predicted by different turbulence models.*

***Table 1**: Initial and boundary conditions used for the simulations*

Mass inlet for	**Hot drying air**
Temperature (K)	478
Mass flow rate (kg/s)	0.03
Turbulent Intensity (%)	5
Hydraulic Diameter (m)	0.075
Mass fraction of H_2O (-)	0.007
Pressure inlet for	**Entrained air**
Gauge total pressure (Pa)	0
Turbulent kinetic energy (m^2s^{-2})	1
Specific dissipation rate (1/s)	1
Mass fraction of H_2O (-)	0.007
Pressure outlet for air	
Vacuum gauge pressure (Pa)	-5
Wall (all)	
Convective heat transfer coefficient ($Wm^{-2}K^{-1}$)	2.5
Free stream temperature (K)	300
Discrete phase (Injection properties)	
Total mass flow rate (kg/s)	0.00083
Temperature (K)	293.15
Rosin-Rammler (RR) Diameter range (µm)	10 – 190
RR- Mean Diameter (µm)	78.5
Spread Parameter (-)	1.33
Number of [diameters, streams] (-)	[10, 20]
Injection type	cone with an angle of 70° and an outer radius of 0.0005 m
Material & Composition	Multicomponent, 10% (by weight) skim milk (not-vaporizing) in water

Table 2: *Comparison of predicted and measured average moisture content (water mass fraction in particle) of the skim milk powder collected at the bottom of the chamber as well as outlet air conditions*

Quantity	Simulation results with turbulence model			Measured
	kε-RNG	kω-SST	kω-SST with modified constants	
Mass weighted average water mass fraction in particle* (%)	47.9	8.13	4.67	5.65 ± 0.12
Humidity ratio of outlet air (wet basis) (g/kg)	17.4 ± 1.2	16.9 ± 0.2	17.2 ± 0.3	18.9 ± 2.7
Outlet temperature (°C)	63.6 ± 2.5	59.6 ± 0.50	58.6 ± 0.44	56.8 ± 1.4

* The equilibrium moisture content of the particle computed from the sorption isotherm using the ambient air conditions was 6.59%. Therefore, this was a clear indication that the particles, which would have experienced hotter air conditions (potentially lower particle equilibrium moisture content) throughout the drying process within the tower, was not in equilibrium with the cooler entrained ambient air, when leaving the bottom outlet of the tower.

***Table 3**: Comparison of the dryer geometry (aspect ratio, expansion ratio) and the Reynolds number among some reported studies in the literature**

Reported in	Inlet hydraulic diameter, $d_{h,i}$ (m)	Diameter ratio chamber:inlet $= d_D/d_{h,i}$ (-)	Chamber length: diameter ratio $= L_D/d_D$ (-)	Chamber Reynolds number, Re_D (-)	Inlet Reynolds Number, Re_i (-)	Turbulence model used
Ullum (2006)	0.013	122.1	1.3	5423	1.66×10^4	k-ω SST
Jaskulski et al. (2015)	0.018	27.9	14.0	10664	7.35×10^3	RSM
Woo et al. (2009a); Woo et al. (2008)	0.040	25.0	1.7	1830	6.35×10^3	k-ε
Bayly et al. (2004)	0.050	24.4 (base)	2.3	34087	1.12×10^5	RSM
	0.102	12.0 (main)			1.63×10^5	
Huang et al. (2004)	0.048	20.8	1.5	1423	6.84×10^3	k-ε, RSM
Jaskulski et al. (2016); Wawrzyniak et al. (2017)	0.433	13.9	4.7	166894	1.12×10^5	RSM
Ullum et al. (2010)	0.200	13.4	1.5	10084	6.25×10^4	k-ω SST
Langrish et al. (2004)	0.070	11.4	2.0	3007	3.78×10^4	k-ω SST
Current case	0.075	8.0 (hot air)	6.7	7804	1.98×10^4	k-ε, k-ω SST
	0.525	1.1 (entrained)			5.41×10^3	
Jaskulski et al. (2017)	0.400	1.0	15.0	257	2.57×10^2	k-ε
Li and Zbicinski (2005)	0.500	1.0	12.0	23855	2.39×10^4	k-ε, RSM

*Since all the minute details pertaining to the dryer system were not always specified explicitly, some missing information to calculate the parameters presented in the table was extracted from the respective publication by means of estimation and was not confirmed by the corresponding authors.